optica

Light localization in optically induced deterministic aperiodic Fibonacci lattices

Martin Boguslawski,[1,*] Nemanja M. Lučić,[2] Falko Diebel,[1] Dejan V. Timotijević,[2] Cornelia Denz,[1] and Dragana M. Jović Savić[2]

[1]Institut für Angewandte Physik and Center for Nonlinear Science (CeNoS), Westfälische Wilhelms-Universität Münster, 48149 Münster, Germany
[2]Institute of Physics, University of Belgrade, P.O. Box 68, 11080 Belgrade, Serbia
*Corresponding author: martin.boguslawski@uni-muenster.de

Received 2 November 2015; revised 2 May 2016; accepted 17 May 2016 (Doc. ID 253058); published 29 June 2016

As light localization becomes increasingly pronounced in photonic systems with less order, we investigate optically induced two-dimensional Fibonacci structures that are supposed to be among the most ordered realizations of deterministic aperiodic patterns. For the generation of corresponding refractive index structures, we implement a recently developed incremental induction method using nondiffracting Bessel beams as waveguide formation entities. Even though Fibonacci structures present slightly reduced order, we show that transverse light transport here is significantly hampered in comparison with discrete diffraction in a periodic lattice. Numerical simulations that support our experimental findings help to identify three cases of input waveguide configurations that significantly determine the initial propagation in a Fibonacci structure. These crucial starting conditions determine the character of light transport, yielding either localization or enhanced expansion. A diverse set of light transport scenarios is identified therein.

OCIS codes: (190.5330) Photorefractive optics; (050.5298) Photonic crystals; (050.1940) Diffraction.

http://dx.doi.org/10.1364/OPTICA.3.000711

1. INTRODUCTION

Order is one of the central properties to characterize complexly structured systems of any dimensionality. There is certainly no doubt that periodic systems hold highest order and, thus, periodicity—meaning the invariance in translation for integer multiples of a set of lattice vectors—has been examined thoroughly over the past centuries, so that there is now a deep theoretical understanding of waves in periodic media. Consequently, universal theories such as Floquet's theorem were introduced. Herein, the model of band structures is a prominent achievement that is frequently recovered in numerous disciplines, for instance, for light propagation in periodically modulated photonic lattices [1,2]. The existence of bandgaps where propagation is forbidden as, per definition, no eigenstates exist within these gaps, is a fundamental awareness in all band-structure systems.

Quasi-periodic structures obviously are of less order than periodic structures as they lack in short-range order [3,4]. However, the spectra of both periodic and quasi-periodic structures present only discrete contributions and are distinguishable by their rotation symmetry at the utmost, which is limited to 2-, 3-, 4-, or 6-fold for periodic lattices. For quasi-periodic structures, even higher rotation symmetry can emerge and, more interestingly, band-structure properties can be assigned to these systems as well, de facto offering complete bandgaps [5,6].

Numerous experimental techniques to achieve refractive index modulations, such as direct laser writing [7] and photolithography techniques [8] have been suggested in past decades [2]. In photorefractive media, for instance, the refractive index is usually modulated by illumination with structured light [9]. In particular, optical induction of elongated two-dimensional (2D) photonic structures can be achieved using so-called nondiffracting beams [10] in which the intensity is modulated transversely while being constant in the direction of propagation [11]. This technique is highly dynamic because the refractive index modulation achieved with low to moderate intensities is reversible and introduces a nonlinear response, which allows for the realization of discrete soliton formations in periodic photonic structures [12,13]. Corresponding to the induction of periodic photonic lattices, the use of quasi-periodic nondiffracting writing beams, such as a fivefold Penrose intensity configuration, allows for the optical generation of according photonic quasi-crystals [14,15].

In general, nondiffracting beams cover an enormous variety of intensity modulations, ranging with decreasing order from periodic [16] to quasi-periodic [11] to random structures [17,18]. Yet, discrete structures without rotation symmetry are barely feasible with a single-beam induction configuration. We thus presented recently that optical induction techniques can be extended to resemble any aperiodic structure by sets of zero-order Bessel beams as waveguide formation entities [19]. By applying this incremental induction technique [20,21], we realized fully aperiodic, so-called Vogel lattices that are prominent examples for

structures inspired by nature, as similar arrangements can be found by plant growth following golden-angle phyllotaxis [22]. Vogel spirals do not show any periodicity in most cases, though they are created deterministically, as a construction rule assembles the structure iteratively up to an arbitrary quantity of elements.

Of course, there are uncountable examples of deterministic aperiodic structures [23] holding different degrees of order [24]. However, in terms of order, the Lebesgue's decomposition theorem was suggested to categorize structures along their spectral appearance [25,26]. Spectra of aperiodic structures with highest order, including Fibonacci patterns [27,28], show only discrete contributions, while low-order structures such as Rudin–Shapiro patterns feature continuous quasi-white-noise spectra [23]. Accordingly, structures with intermediate order have both singular and continuous spectral properties. The most famous structure among them certainly arises from the Thue–Morse sequence [24].

The question of how an altering degree of order influences wave (or light) propagation remains untouched within this categorization scheme. As localization in the sense of reduced light transport becomes more significant in disordered photonic systems [29–31], the occurrence of localized modes due to a deterministic aperiodicity is ascribed to flat bands along with bandgaps that unclose with decreased order [5]. In consequence, finding signatures of localization already in singular-spectral structures would directly refer to an expected reduced degree of order in comparison to periodic lattices with likewise singular spectra.

In this contribution, we examine waveguide patterns of pure-point spectra by exploring light localization effects [32,33] in optically induced refractive index Fibonacci structures [28]. In contrast to transmission measurements in one-dimensional (1D) Fibonacci multilayer experiments [34], we examine transport characteristics in 2D Fibonacci systems per broad spectral excitation. Compared to similar experiments in 1D waveguide Fibonacci structures [33], we expect a higher diversity of transport characteristics due to the extended dimensionality and additional degree of freedom. We adapt the nomenclature localization to explain suppressed transport in quasi-periodic [14] and aperiodic structures, not to be confused with Anderson localization [35] appearing in disordered lattices.

Experimentally, we benefit from a highly dynamic and reversible induction scheme at realizing largely elongated 2D photonic structures that offer excellent interaction distances. In Fibonacci arrangements, diverse local configurations of lattice sites exist. Hence, we consider an output average for waveguide excitation at different input positions. By comparing our results with a periodic photonic lattice configuration where discrete diffraction with a high rate of transport is expected to be found [7], we underline that order is significantly diminished already in aperiodic structures with pure-point spectra, hampering light transport and causing localization [34].

Besides examining average outputs, we also put a focus on single light-transport scenarios and identify both localized and extended states depending on the initial condition of the input-waveguide surrounding. It has been shown before that in quasi-periodic structures the degree of (light) transport and localization strongly depends on the input position, e.g., in a Penrose pattern [14,15], though in these publications, not much attention has been paid to analyze this influence in very detail. The Fibonacci pattern is particularly appropriate, as there are only few scenarios of input conditions, but aperiodicity plays a leading role for longer propagation distances.

The manuscript is structured as follows. First, we present our approach of applying 1D Fibonacci words to create 2D lattices with Fibonacci tiling. After we have described the applied experimental techniques and specific parameters that we used for the optical induction, we present our results of single-waveguide excitation and compare these experimental data with numerical simulations. Finally, we cross check our results against light propagation events in a regular lattice before a conclusion is drawn in the last section.

2. DESIGN AND INDUCTION OF 2D FIBONACCI LATTICES

Our approach to designing an aperiodic Fibonacci pattern is to vary the distances of adjacent waveguides encoded as Fibonacci words [28]. These sequences are binary, and according to the Fibonacci series, the nth word is generated by combining the $(n-1)$st and the $(n-2)$nd word, such as $\mathcal{S}_n = \{\mathcal{S}_{n-1}\mathcal{S}_{n-2}\}$. Giving the first two words determines the complete set of all words. We define two different distances $\mathcal{A}$ and $\mathcal{B} = \mathcal{A}/\varphi$, where $\varphi = (1+\sqrt{5})/2$ is the golden ratio, and set $\mathcal{S}_0 = \mathcal{A}$ and $\mathcal{S}_1 = \mathcal{AB}$ such that the first five Fibonacci words read as

$$\mathcal{S}_0 = \mathcal{A}, \qquad \mathcal{S}_1 = \mathcal{AB}, \qquad \mathcal{S}_2 = \mathcal{ABA},$$
$$\mathcal{S}_3 = \mathcal{ABAAB}, \qquad \mathcal{S}_4 = \mathcal{ABAABABA}.$$

By picking two sub-words of length N from a very long Fibonacci word $\mathcal{S}_n$ with $n \gg N$ starting at arbitrary but different elements for two transverse directions, we receive a deterministic aperiodic, nonsymmetric structure with $N \times N$ sites, as depicted in Fig. 1(a). Here, the typical character of a Fibonacci word is present in both orthogonal directions. That is, distance $\mathcal{A}$ occurs with a probability of $\varphi - 1 = 0.62$, thus more frequently than $\mathcal{B}$, which yields typical structure groups: quad, double, and single waveguide elements [28].

The Fourier transform of the Fibonacci structure shown in Fig. 1(a) gives the spatial spectrum whose absolute value distribution $S(k_x, k_y)$ is presented in Fig. 1(b). The singular character becomes apparent here, but especially in Fig. 1(e), where the orange plot represents the cross-section distribution $S(k_t)$ along the arrow in Fig. 1(b). For comparison, the corresponding plot for a largely extended Fibonacci grating and, thus, with extensive resolution, is given by the black curve. Notice that particular frequency peaks have mutual distance relations equal to the golden ratio φ. Frequencies with distinct amplitude peaks can be found at $k_t = \varphi^m \kappa$, where κ is the frequency of the prominent peak settled between $\pi/\mathcal{A}$ and $\pi/\mathcal{B}$, and m is a natural number. Thus, in addition to the nomenclature aperiodic, a classification of the presented spectrum as singular or pure-point is appropriate, as well [26].

After we have determined the waveguide positioning scheme resembling a 2D Fibonacci arrangement, we apply the incoherent-Bessel beam induction method to preserve the nondiffracting character of the effective intensity during the writing process. This method implies that every single waveguide is written with an appropriate nondiffracting Bessel beam of zeroth order and structural size. Determining the structural size of the Bessel beam intensity settles the waveguide diameter. In our considerations, the full width at half-maximum of a Bessel beam intensity is

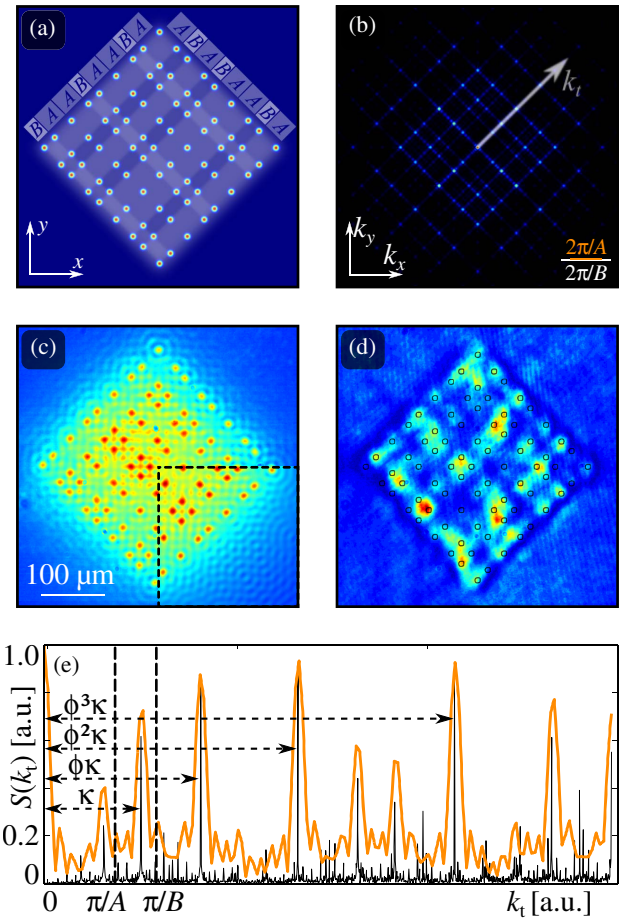

Fig. 1. (a) Fibonacci lattice with Gaussian beam sites (underlying Fibonacci words indicated alongside). (b) Spatial spectrum $S(k_x, k_y)$ according to lattice shown in (a). (c) Measured effective intensity with Bessel beam lattice sites taken by multiple-shot illumination at the back face of the crystal. Bottom right quadrant shows according numerical simulation. (d) Experimental output for plane-wave probing (contours indicate waveguide positions). (e) Plot of (orange) spectrum $S(k_t)$ along the direction denoted in (b) and of (black) the ideal spectrum for an extended aperiodic Fibonacci lattice with δ-function lattice sites.

determined to 9.3 μm and the effective waveguide distance to be $d_{\text{eff}} = 32$ μm. This yields $\mathcal{A} = 37.5$ μm and $\mathcal{B} = 23.2$ μm. A simulation of the resulting transverse effective intensity distribution is given in the lower right quadrant of Fig. 1(c).

In general, our experimental setup that incorporates a set of spatial light modulators (SLMs) is appropriate to generate any kind of (nondiffracting) beam [11]. The respective setup scheme is presented in Fig. 2, and the induction process corresponds to descriptions given in Ref. [19]. We use the SLMs to experimentally realize numerically calculated light fields in a particular image plane defined by an optical imaging system with a demagnification factor of roughly 1/6. Particularly, the phase-only SLM (PSLM; Holoeye Pluto) is positioned in real space (related to the image plane) in order to modulate incoming plane waves. The entire field information of the desired beam is encoded in elaborate diffraction gratings displayed by the PSLM. An amplitude-only SLM (ASLM; Holoeye LC-R 2500) is placed in Fourier space for spectral low-pass filtering reasons. For all experiments, we use a frequency-doubled Nd:YAG continuous-wave laser source at 532 nm wavelength.

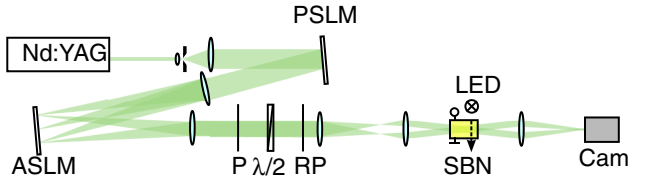

Fig. 2. Experimental setup for induction of Fibonacci lattices with incoherent Bessel beams. (A/P)SLM, (amplitude/phase) spatial light modulator; Cam, CCD camera; $\lambda/2$, half-wave plate; LED, background illumination; (R)P, (rotatable) polarizer; SBN, strontium barium niobate crystal; lenses and pin hole not labeled.

To resemble the desired 9 × 9 Fibonacci structure as presented in Fig. 1(a), we basically change the position of each Bessel writing beam and put its central maximum to the defined position resulting from the given structure design. A full set of diffraction gratings containing the necessary writing light fields is generated by convolution of a sparse matrix (with the entire position information) and a basic Bessel beam field distribution.

For the actual experimental induction, it is sufficient to send every Bessel beam diffraction grating sequentially to the SLM, each generating a corresponding light intensity in the volume of interest where a photorefractive strontium barium niobate (SBN:60) crystal is placed; the crystal is doped with cerium [36]. During the illumination, an external field of 2 kV cm^{-1} is applied to the crystal [9]. This sequential induction scheme implies an effectively incoherent superposition of all writing light fields of one set. The obvious motivation is that a coherent overlap of contributing Bessel beams would cause undesired intensity modulations since off-diagonal terms of the resulting field would be nonzero. However, by introducing an effective intensity I_{eff}, we aim to implement the sum of all intensities $I_{\text{eff}} = \Sigma_k I_k = \Sigma_k |E_k|^2$ rather than the absolute square of all fields $|\Sigma_k E_k|^2$.

Simulated and experimental effective intensities are given in Fig. 1(c). The intensity distributions of writing and probing light fields are recorded by a CCD camera imaging system. To receive the experimental picture, the output intensity of each writing beam is taken individually and added up afterward. This overall intensity pattern displays the effective intensity that optically induces the 2D photonic structure. A LED is placed above the crystal to actively erase inscribed structures for further light potential inductions.

Figure 1(d) shows the output intensity when probing the induced structure with a plane wave. Note that waveguide positions of quad and double elements cannot be resolved properly here, as one intensity envelope covers clusters of adjacent waveguides for predominantly perpendicular probe beam incidence. However, we will see later on that single waveguide excitation indicates accurate induction of waveguide groups according to the effective intensity distribution.

3. TRANSPORT CHARACTERISTICS IN A FIBONACCI LATTICE

After induction, we experimentally investigate the influence of the Fibonacci lattice with its diverse local conditions on the beam propagation in the linear regime of low probing beam power of several μW, and compare our experimental results with numerical simulations. To numerically model light propagation

along the z direction of any photonic lattice, we consider the paraxial wave equation

$$\{2ik\partial_z + \Delta_\perp - kn_e^2 r_{33}(\partial_x \Phi_{sc})\}A(\vec{r}) = 0 \quad (1)$$

for a slowly varying electric field amplitude $A(\vec{r})$ with wave number k. In this equation, ∂_{x_i} is the spatial derivation in the x_i direction, $\Delta_\perp$ the transverse Laplacian perpendicular to z, n_e the unmodulated refractive index for extraordinary polarization, r_{33} the corresponding electro-optical coefficient, and Φ_{sc} denotes a light potential caused by the optically induced internal electric field that in our case holds the Fibonacci structure. To simulate light propagation, we choose parameters that match experimental conditions and use a split-step method to evaluate the wave equation. Typical refractive index contrasts in the vicinity of a lattice site extracted from numerical calculations are 3×10^{-5}, consistent with experimental conditions. We do not achieve maximally feasible modulations of 10^{-4} due to the background intensity modulation between lattice sites as given in Fig. 1(c).

For light-transport studies, a Gaussian probe beam of $w_0 = 14$ μm beam waist is launched at different input positions of a Fibonacci photonic lattice. Figure 3 shows five particular output results of light propagation through a lattice of 20 mm propagation length. The specific input positions on and between lattice sites are labeled from 1 to 5 in Fig. 3(k) and are related to output distributions shown in the first to fifth columns in Fig. 3 as indicated. Top-row images Figs. 3(a)–3(e) present typical output distributions experimentally observed at the exit face of the crystal, while the bottom row [Figs. 3(f)–3(j)] represents the corresponding distributions obtained numerically.

We notice very good agreement between experimentally obtained and numerically simulated results. Naturally, the separation between incident and neighboring lattice sites has a very strong influence on the propagation process as the coupling coefficients vary inversely to their spacing [7]. Thereby, light is subject to be guided along waveguide lattice sites accompanied by coupling between adjacent waveguides, as well as to ballistic propagation for predominantly high spatial frequencies encountering low spectral amplitudes [cf. Fig. 1(b)].

Moreover, a pronounced heterogeneity of output profiles for different initial positions can be found in Figs. 3(a)–3(e), indicating that the appearance of excited modes is highly diverse. We distinguish three cases originating from the initial conditions of the specific input-waveguide environment as summarized in Fig. 4. The underlying numerical calculations consider a 30×30 lattice site arrangement in order to avoid surface influences. A particular Fibonacci structure is determined by choosing randomly the two orthogonal Fibonacci words, allowing us to statistically analyze individual input configurations. One configuration is characterized by an isolated waveguide with next sites separated by $\mathcal{A}$, as sketched in Fig. 4(a) for $z = 20$ mm, similar to Figs. 3(c) and 3(h). For even longer propagation distances, two diagonal lines of low intensity are characteristic, as documented in Figs. 4(b) and 4(c) for two different realizations of this scenario.

The second input configuration consisting of a double-waveguide input area is given in Fig. 4(d) [cf. Figs. 3(b) and 3(g)]. After sufficiently long propagation, one diagonal low-intensity line establishes for this input constellation as observed for the two realizations presented in Figs. 4(e) and 4(f).

Corresponding to Figs. 3(a) and 3(f), the third case we want to distinguish is given by a quad group of waveguides with one site acting as the input waveguide. This arrangement is indicated in Fig. 4(g) together with the intensity distribution for 20 mm propagation. In Figs. 4(h) and 4(i), we identify that, after 60 mm, a considerable amount of light is confined around the quad-waveguide input group.

For a more quantitative analysis, we introduce with the effective beam width $\omega_{eff}(z) = P(z)^{-1/2}$ a usual measure to characterize the degree of light confinement, where

$$P(z) = \frac{\int |E(x,y,z)|^4 dxdy}{\left(\int |E(x,y,z)|^2 dxdy\right)^2} \quad (2)$$

is the inverse participation ratio [29].

By studying how the effective beam width develops with increasing propagation distance, we directly identify the heterogeneity of propagation states. To extract an averaged effective beam width ω_{mean}, we take the arithmetic mean of effective beam widths for 50 different on-site input positions, each corresponding to one potential realization. Accordingly, in Fig. 5(a) absolute effective beam widths of 50 simulated propagation scenarios are plotted against the distance $z \leq 80$ mm.

While all effective beam widths are almost equal for the first 10 mm, separation starts for longer propagation distances, since coupling arises to next-nearest waveguides referring to the input.

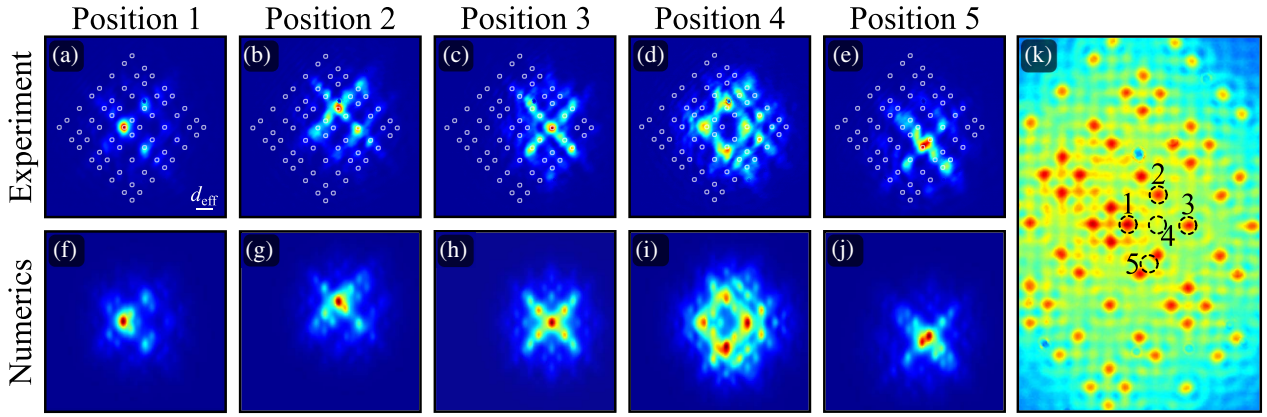

Fig. 3. Light propagation in aperiodic Fibonacci photonic lattices. Intensity distributions at the exit face of the crystal experimentally observed (first row) and numerically calculated (second row) for input probe beam size $w_0 = 14$ μm. Columns correspond to input beam positions 1 to 5, as shown in (k).

At this point, the aperiodic character of the Fibonacci structure comes into play at the earliest.

For the experimentally feasible propagation distance of 20 mm, we observe an increase of $\omega_{\mathrm{eff}}(z)$ by a factor within the range of 7 to 8. Here, we find a significant split-up of the beam widths in conformity with distributions documented in Figs. 3 and 4. Plotting the relative beam widths $\omega_{\mathrm{eff}}(z)/\omega_{\mathrm{mean}}$, as presented in Fig. 5(b), gives more insight into diverse transport characteristics for individual input arrangement scenarios.

The corresponding single-waveguide branch in Fig. 5(b) is in red and represents the broadest beam widths along the considered distance [cf. Fig. 4(a)]. Among the 50 randomly chosen Fibonacci potentials, this case occurred four times, yielding rather comparable beam widths. The statistical probability of finding an isolated-waveguide input is $p_{\mathcal{A}\mathcal{A}|\mathcal{A}\mathcal{A}} \approx 6\%$. In this notation, the indices indicate the distances around the central waveguide in both orthogonal directions, separated by the vertical bar.

The green branch in Fig. 5(b) gives the beam widths for a double-waveguide input as indicated in Fig. 4(d). This is one of four possible double-waveguide configurations that emerge from 90° rotations of the underlying structure around the input waveguide. Generally, these initial conditions yield beam widths above average and contribute to the maximum beam width at $z = 80$ mm. This case is found among 23 of the 50 Fibonacci structures. However, the corresponding probability is $p_{\mathcal{A}\mathcal{B}|\mathcal{A}\mathcal{A}} \approx 36\%$. Here, permuting indices within one dimension covers the same case.

Though the fastest initial beam broadening is found for $z < 15$ mm among the quad-waveguide input configuration, this arrangement mainly yields beam widths below average. The corresponding branch is in purple in Fig. 5(b), and the configuration has a probability of $p_{\mathcal{A}\mathcal{B}|\mathcal{A}\mathcal{B}} = 58\%$. Here as well, we associate all four cases arising from multiple 90° rotations of such structures, as indicated in Fig. 4(g). The beam width deviation, however, is remarkably large among all observed 23 quad-group cases. Equivalently, we find in Fig. 5(b) one trend that is comparable with the maximum case at $z = 80$ mm. Yet, the smallest beam width arises from this quad-group starting condition, as well.

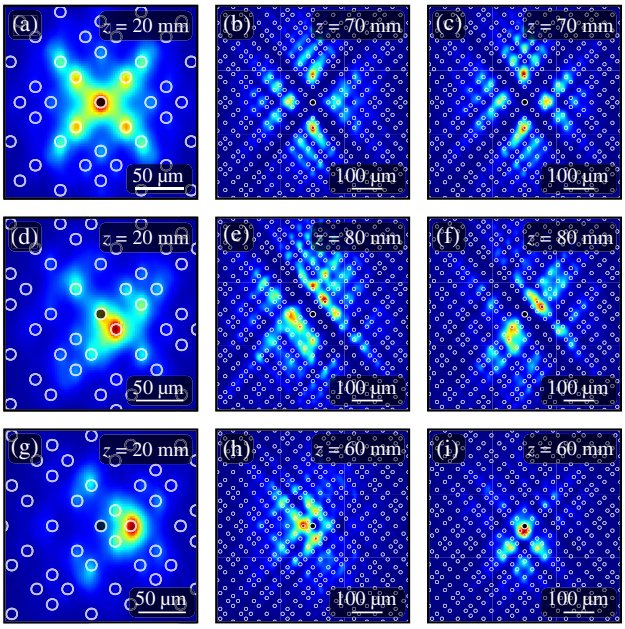

Fig. 4. Three cases of input waveguide configuration. Computed images show intensity distributions of (top row) single-, (middle row) double-, and (bottom row) quad-waveguide input for particular propagation distances as indicated in the upper right corner and marked in Fig. 5(b). Filled circles mark the position of the input waveguide.

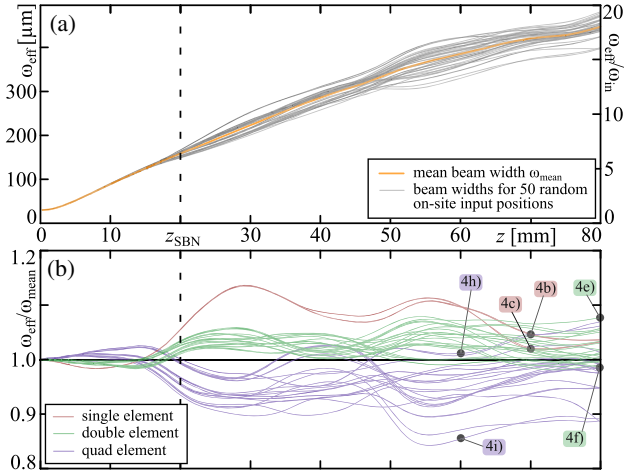

Fig. 5. Development of beam widths with propagation distance. (a) Absolute beam widths ω_{eff} of individual on-site probing scenarios and mean of beam width ω_{mean}. (b) Relative beam widths $\omega_{\mathrm{eff}}/\omega_{\mathrm{mean}}$. Labels in (b) identify images in Fig. 4.

In consequence, for a short propagation distance, we can identify the input condition out of the three cases directly by the shape of the intensity distribution. For $z > 50$ mm, the effective beam-width lines of all three input cases interlace and merge increasingly, yielding a heterogeneous set of light transport scenarios. Here, individual light potential configurations facilitate extreme cases of maximum or minimum beam widths. It is, however, the initial waveguide configuration that mainly affects the width of the intensity distribution.

Moreover, in Fig. 5(b), we also find lines that overlap for long distances, even along the full considered distance of 80 mm, before splitting up. The split-up of the red branch (isolated waveguide input) at ≈38 mm is representative, although, particularly here, four lines divide into two double lines. It can be understood by the Fibonacci word characteristics that these lines overlie for such a long distance. Along with an isolated input site occurs a definite surrounding of diameter of seven waveguides around this site. The fixed sequence in both directions inside this area is $\mathcal{A}\mathcal{B}\mathcal{A}\mathcal{A}\mathcal{B}\mathcal{A}$. Beyond this sequence, the distances can either be $\mathcal{A}$ or $\mathcal{B}$, again.

Generally, we can specify that, for two overlapping $\omega_{\mathrm{eff}}(z)$ lines, the underlying potentials are indistinguishable within a transverse area around the input position. Beyond this area, a difference between both considered potentials appears and propagation conditions vary. In this context, two Fibonacci potentials differ locally in at least one of the two orthogonal directions by means of permuting the combination $\mathcal{A}\mathcal{B}$ to $\mathcal{B}\mathcal{A}$ or vice versa. Consequently, a spatially resolved comparison of two unknown, but deterministic aperiodic, Fibonacci potentials would be very simple in this scheme and applicable to according deterministic aperiodic structures.

4. COMPARISON WITH BEAM PROPAGATION IN PERIODIC LATTICES

To evaluate the strength of light localization in a Fibonacci structure, we experimentally compare this kind of deterministic aperiodic lattice with the periodic case, both of 20 mm length. Last named lattices are arranged periodically with as many lattice sites as for the aperiodic case, using again the sequential Bessel beam writing technique to preserve comparability. For this geometry, the lattice period corresponds to the effective distance of the Fibonacci lattice, $d = 32$ μm. The experimental effective intensity, the plane-wave probing output, and the waveguide-excitation output are shown in Figs. 6(a)–6(c), respectively. Again, probing the structure with a plane wave does not resolve the light potential in much detail, as can be found in Fig. 6(b), although the image indicates qualitatively the area of modulated refractive index. A Gaussian beam of $w_0 = 14$ μm exciting the central lattice point reveals the typical discrete diffraction at the output face, as given in Fig. 7(c), and is expected for regular lattices [7].

We further numerically study the beam propagation in Fibonacci and regular photonic lattices along $z \leq 80$ mm with respect to the development of the probe beam width, including the experimental case of $z = 20$ mm.

Figure 7 allows comparison of our numerical results of beam propagation in aperiodic Fibonacci photonic lattices against the periodic lattice case and a homogeneous medium without refractive index modulation. In Fig. 7(a), the averaged effective beam width $\omega_{\text{mean}}(z)$ and $\omega_{\text{eff}}(z)$ for Fibonacci, periodic lattice, and a homogeneous medium are presented. The initial Gaussian beam waist $w_0 = 14$ μm corresponds to $\omega_{\text{eff}}(z = 0) \approx 25$ μm. Both photonic structures show transport that is below beam broadening in a homogeneous medium. Moreover, results in Fig. 7(a) indicate that the Gaussian input expands significantly more slowly during propagation in Fibonacci lattices than under periodic conditions. We additionally plotted two extreme transport scenarios to show the variance of beam expansion in contrast to the discrete diffraction case. Remarkably, light transport can temporally be faster than discrete diffraction, as observed for $z \approx 30$ mm. This enhanced transport originates from the single-waveguide input configuration [cf. Fig. 4(a)].

The averaged output intensity distribution after 70 mm of propagation in Fibonacci lattices is given in Fig. 7(b). Figures 7(c) and 7(d) present the output in a periodic lattice and in a homogeneous medium, respectively. A typical signature of discrete diffraction is prominent for the square lattice. Interestingly, the median intensity distribution in the Fibonacci structure features an underlying modulation similar to the discrete diffraction signature.

Nevertheless, diffraction is essentially suppressed in comparison with periodic lattices, and localization in Fibonacci lattices is

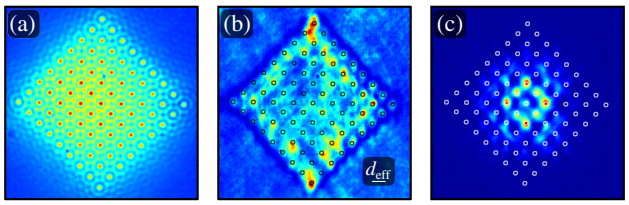

Fig. 6. Experimental images for a periodic photonic square lattice. (a) Effective intensity, (b) plane-wave, and (c) single-site probing output.

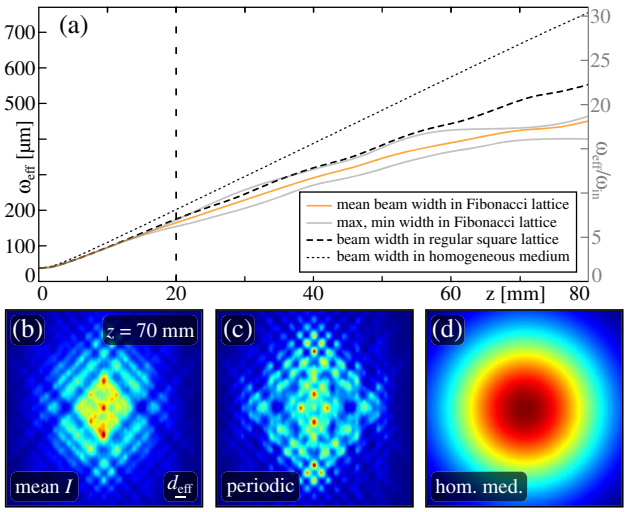

Fig. 7. Comparison of effective beam width development in a Fibonacci lattice against periodic and homogeneous medium cases. (a) Beam widths ω_{eff} versus propagation distance z: (orange) mean beam width ω_{mean}, and (gray) individual beam width; beam width in (dashed black) a periodic lattice and (dotted black) a homogeneous medium. Dashed vertical line at $z = 20$ mm indicates experimental propagation distance. Intensity distributions at $z = 70$ mm in (b) averaged Fibonacci intensity, (c) periodic square lattice, and (d) homogeneous medium, each for $w_0 = 14$ μm.

present, as the highest intensity is predominantly located around the input center. Consequently, transverse light transport is slowed down on average due to aperiodic conditions accounting for localized modes whose appearance indirectly indicate the presence of bandgaps [23]. Periodic structures, in contrast, bring forward extended propagation modes, as more light is carried away from the input position due to discrete diffraction.

5. DISCUSSION AND CONCLUSIONS

To conclude, we have observed light localization in optically induced 2D Fibonacci photonic lattices that arises from the aperiodic waveguide arrangement. By experimentally and numerically analyzing linear propagation characteristics for various incident positions, we observed enhanced localization in Fibonacci photonic lattices compared with discrete diffraction-driven light transport in equivalent periodic realizations. We identify this localization with the occurrence of localized modes due to aperiodic structural conditions with diminished order, indirectly indicating the existence of bandgaps.

A very good agreement between experimental and numerical results allowed us to additionally analyze the development during propagation of a wave packet sent to corresponding lattices. The individual configuration of waveguides around the input site gives diversified starting conditions and crucially determines further transport properties of the photonic structure. By means of an effective beam width, we identified a very heterogeneous set of propagation states that inherently stems from the aperiodic character of the Fibonacci structure. Besides conditions that reduce light transport, we also identified single scenarios of enhanced excitation that temporarily can be above discrete-diffraction transport. Evidently, the shape of excited localized modes and, thus, the strength of localization, are local rather than global properties

in the kinds of structures that have been the subject of our investigations.

Moreover, the numerical results consolidated our experimental observations and gave deeper insights into propagation dynamics. Additional investigations on this exciting aperiodic structure that would go beyond the scope of this manuscript might be the influence of additional disorder or nonlinear light–matter interaction. Analyzing beam excitation scenarios and light transport in other aperiodic structures of less order would directly identify the influence of the degree of order of a photonic structure. Topology would be another interesting issue to be investigated when bringing together different kinds of quasi- or aperiodic structures [37]. A 2D implementation of proper structural boundaries is directly feasible with our experimental technique.

In general, we are convinced that our results can be transferred to other kinds of aperiodic refractive index lattices, using the presented ideas and methods.

Funding. German Academic Exchange Service (DAAD) (56267010); Ministry of Education, Science and Technological Development, Republic of Serbia (OI 171036).

Acknowledgment. We acknowledge support by the Open Access Publication Fund of the University of Münster.

REFERENCES

1. P. St. J. Russell, "Optics of Floquet-Bloch waves in dielectric gratings," Appl. Phys. B **39**, 231–246 (1986).
2. J. D. Joannopoulos, S. G. Johnson, J. N. Winn, and R. D. Meade, *Photonic Crystals: Molding the Flow of Light*, 2nd ed. (Princeton University, 2008).
3. D. Shechtman, I. Blech, D. Gratias, and J. W. Cahn, "Metallic phase with long-range orientational order and no translational symmetry," Phys. Rev. Lett. **53**, 1951–1953 (1984).
4. D. Levine and P. J. Steinhardt, "Quasicrystals: a new class of ordered structures," Phys. Rev. Lett. **53**, 2477–2480 (1984).
5. Y. S. Chan, C. T. Chan, and Z. Y. Liu, "Photonic band gaps in two-dimensional photonic quasicrystals," Phys. Rev. Lett. **80**, 956–959 (1998).
6. M. Florescu, S. Torquato, and P. J. Steinhardt, "Complete band gaps in two-dimensional photonic quasicrystals," Phys. Rev. B **80**, 155112 (2009).
7. T. Pertsch, U. Peschel, F. Lederer, J. Burghoff, M. Will, S. Nolte, and A. Tünnermann, "Discrete diffraction in two-dimensional arrays of coupled waveguides in silica," Opt. Lett. **29**, 468–470 (2004).
8. M. Campbell, D. N. Sharp, M. T. Harrison, R. G. Denning, and A. J. Turberfield, "Fabrication of photonic crystals for the visible spectrum by holographic lithography," Nature **404**, 53–56 (2000).
9. H. Trompeter, W. Krolikowski, D. N. Neshev, A. S. Desyatnikov, A. A. Sukhorukov, Y. S. Kivshar, T. Pertsch, U. Peschel, and F. Lederer, "Bloch oscillations and Zener tunneling in two-dimensional photonic lattices," Phys. Rev. Lett. **96**, 053903 (2006).
10. J. Durnin, "Exact solutions for nondiffracting beams. I. The scalar theory," J. Opt. Soc. Am. A **4**, 651–654 (1987).
11. P. Rose, M. Boguslawski, and C. Denz, "Nonlinear lattice structures based on families of complex nondiffracting beams," New J. Phys. **14**, 33018 (2012).
12. D. N. Christodoulides, F. Lederer, and Y. Silberberg, "Discretizing light behaviour in linear and nonlinear waveguide lattices," Nature **424**, 817–823 (2003).
13. F. Lederer, G. I. Stegeman, D. N. Christodoulides, G. Assanto, M. Segev, and Y. Silberberg, "Discrete solitons in optics," Phys. Rep. **463**, 1–126 (2008).
14. B. Freedman, G. Bartal, M. Segev, R. Lifshitz, D. N. Christodoulides, and J. W. Fleischer, "Wave and defect dynamics in nonlinear photonic quasicrystals," Nature **440**, 1166–1169 (2006).
15. L. Levi, M. Rechtsman, B. Freedman, T. Schwartz, and M. Segev, "Disorder-enhanced transport in photonic quasicrystals," Science **332**, 1541–1544 (2011).
16. M. Boguslawski, P. Rose, and C. Denz, "Increasing the structural variety of discrete nondiffracting wave fields," Phys. Rev. A **84**, 13832 (2011).
17. M. Boguslawski, S. Brake, J. Armijo, F. Diebel, P. Rose, and C. Denz, "Analysis of transverse Anderson localization in refractive index structures with customized random potential," Opt. Express **21**, 31713 (2013).
18. S. Brake, M. Boguslawski, D. Leykam, A. S. Desyatnikov, and C. Denz, "Observation of transverse coherent backscattering in disordered photonic structures," arXiv:1501.04458 (2015).
19. F. Diebel, P. Rose, M. Boguslawski, and C. Denz, "Optical induction scheme for assembling nondiffracting aperiodic Vogel spirals," Appl. Phys. Lett. **104**, 191101 (2014).
20. M. Boguslawski, A. Kelberer, P. Rose, and C. Denz, "Multiplexing complex two-dimensional photonic superlattices," Opt. Express **20**, 27331–27343 (2012).
21. M. Boguslawski, A. Kelberer, P. Rose, and C. Denz, "Apodized structures for the integration of defect sites into photonic lattices," Appl. Phys. Lett. **105**, 111102 (2014).
22. J. Trevino, S. F. Liew, H. Noh, H. Cao, and L. Dal Negro, "Geometrical structure, multifractal spectra and localized optical modes of aperiodic Vogel spirals," Opt. Express **20**, 3015–3033 (2012).
23. L. Dal Negro and S. V. Boriskina, "Deterministic aperiodic nanostructures for photonics and plasmonics applications," Laser Photon. Rev. **6**, 178–218 (2012).
24. M. Baake and U. Grimm, "Mathematical diffraction of aperiodic structures," Chem. Soc. Rev. **41**, 6821–6843 (2012).
25. H. Hiramoto and M. Kohmoto, "Electronic spectral and wavefunction properties of one-dimensional quasiperiodic systems: a scaling approach," Int. J. Mod. Phys. B **6**, 281–320 (1992).
26. E. Maciá, "The role of aperiodic order in science and technology," Rep. Prog. Phys. **69**, 397–441 (2006).
27. G. Gumbs and M. K. Ali, "Dynamical maps, Cantor spectra, and localization for Fibonacci and related quasiperiodic lattices," Phys. Rev. Lett. **60**, 1081–1084 (1988).
28. R. Lifshitz, "The square Fibonacci tiling," J. Alloys Compd. **342**, 186–190 (2002).
29. T. Schwartz, G. Bartal, S. Fishman, and M. Segev, "Transport and Anderson localization in disordered two-dimensional photonic lattices," Nature **446**, 52–55 (2007).
30. Y. Lahini, R. Pugatch, F. Pozzi, M. Sorel, R. Morandotti, N. Davidson, and Y. Silberberg, "Observation of a localization transition in quasiperiodic photonic lattices," Phys. Rev. Lett. **103**, 013901 (2009).
31. D. M. Jović, M. R. Belić, and C. Denz, "Transverse localization of light in nonlinear photonic lattices with dimensionality crossover," Phys. Rev. A **84**, 043811 (2011).
32. M. Renner and G. von Freymann, "Transverse mode localization in three-dimensional deterministic aperiodic structures," Adv. Opt. Mater. **2**, 226–230 (2014).
33. N. M. Lučić, D. M. Jović Savić, A. Piper, D. Ž. Grujić, J. M. Vasiljević, D. V. Pantelić, B. M. Jelenković, and D. V. Timotijević, "Light propagation in quasi-periodic Fibonacci waveguide arrays," J. Opt. Soc. Am. B **32**, 1510–1513 (2015).
34. W. Gellermann, M. Kohmoto, B. Sutherland, and P. C. Taylor, "Localization of light waves in Fibonacci dielectric multilayers," Phys. Rev. Lett. **72**, 633–636 (1994).
35. A. Lagendijk, B. Tiggelen, and D. S. Wiersma, "Fifty years of Anderson localization," Phys. Today **62**(8), 24–29 (2009).
36. R. A. Vazquez, M. D. Ewbank, and R. R. Neurgaonkar, "Photorefractive properties of doped strontium-barium niobate," Opt. Commun. **80**, 253–258 (1991).
37. M. Verbin, O. Zilberberg, Y. Lahini, Y. E. Kraus, and Y. Silberberg, "Topological pumping over a photonic Fibonacci quasicrystal," Phys. Rev. B **91**, 064201 (2015).